Journal of Inflammation Research

Dovepress
open access to scientific and medical research

Open Access Full Text Article

ORIGINAL RESEARCH

Exploring Dysregulated Ferroptosis-Related Genes in Septic Myocardial Injury Based on Human Heart Transcriptomes: Evidence and New Insights

Hua-Xi Zou[1,2,*], Tie Hu[1,2,*], Jia-Yi Zhao[2,3,*], Bai-Quan Qiu[2,4], Chen-Chao Zou[2,4], Qi-Rong Xu[1], Ji-Chun Liu[1,2], Song-Qing Lai[1,2], Huang Huang[1,2]

[1]Department of Cardiovascular Surgery, The First Affiliated Hospital of Nanchang University, Nanchang, People's Republic of China; [2]Institute of Cardiovascular Diseases, Jiangxi Academy of Clinical Medical Sciences, The First Affiliated Hospital of Nanchang University, Nanchang, People's Republic of China; [3]Medical Innovation Experimental Program, Huan Kui College, Nanchang University, Nanchang, People's Republic of China; [4]Department of Cardiovascular Surgery, The Second Affiliated Hospital of Nanchang University, Nanchang, People's Republic of China

*These authors contributed equally to this work

Correspondence: Huang Huang; Song-Qing Lai, Email jack19871212@hotmail.com; ndyfy03743@ncu.edu.cn

Introduction: Sepsis is currently a common condition in emergency and intensive care units, and is defined as life-threatening organ dysfunction caused by a dysregulated host response to infection. Cardiac dysfunction caused by septic myocardial injury (SMI) is associated with adverse prognosis and has significant economic and human costs. The pathophysiological mechanisms underlying SMI have long been a subject of interest. Recent studies have identified ferroptosis, a form of programmed cell death associated with iron accumulation and lipid peroxidation, as a pathological factor in the development of SMI. However, the current understanding of how ferroptosis functions and regulates in SMI remains limited, particularly in the absence of direct evidence from human heart.

Methods: We performed a sequential comprehensive bioinformatics analysis of human sepsis cardiac transcriptome data obtained through the GEO database. The lipopolysaccharide-induced mouse SMI model was used to validate the ferroptosis features and transcriptional expression of key genes.

Results: We identified widespread dysregulation of ferroptosis-related genes (FRGs) in SMI based on the human septic heart transcriptomes, deeply explored the underlying biological mechanisms and crosstalks, followed by the identification of key functional modules and hub genes through the construction of protein-protein interaction network. Eight key FRGs that regulate ferroptosis in SMI, including HIF1A, MAPK3, NOX4, PPARA, PTEN, RELA, STAT3 and TP53, were identified, as well as the ferroptosis features. All the key FRGs showed excellent diagnostic capability for SMI, part of them was associated with the prognosis of sepsis patients and the immune infiltration in the septic hearts, and potential ferroptosis-modulating drugs for SMI were predicted based on key FRGs.

Conclusion: This study provides human septic heart transcriptome-based evidence and brings new insights into the role of ferroptosis in SMI, which is significant for expanding the understanding of the pathobiological mechanisms of SMI and exploring promising diagnostic and therapeutic targets for SMI.

Keywords: septic myocardial injury, ferroptosis, heart transcriptome, key genes, database

Introduction

Sepsis, one of the leading causes of death in critically ill patients worldwide, is a life-threatening organ dysfunction caused by a dysregulated host response to infection.[1,2] Although the prognosis of sepsis patients has improved with the development of therapeutic measures such as intensive care and antibiotic application, it is still considered a major public health problem with significant health care and social impact due to the high morbidity and mortality.[3–5] The pathogenesis of sepsis is complex, and not only involves systemic inflammation but also dysfunction of multiple organs.[1] Cardiac dysfunction caused by septic myocardial injury (SMI) is a common and lethal manifestation of sepsis, and is associated with septic shock and increased mortality.[6,7] Clinical and pathological research related to SMI is progressing worldwide,

Received: 7 December 2022
Accepted: 25 February 2023
Published: 9 March 2023

however, there is still a lack of characteristic biomarkers and precise clinical diagnostic and therapeutic strategies.[8–11] Therefore, it is crucial to elucidate the molecular basis of SMI to identify promising targets for its prevention, diagnosis and treatment.[12]

Disruption in iron homeostasis is one of the critical pathological features of sepsis and SMI, and entails increased iron transport and uptake into cells and decreased iron export.[13,14] There is evidence of iron homeostasis disorder in both circulating blood and organ tissues of septic patients, which has been found to be related to the clinical prognosis.[15–17] Since ferroportin is the only known iron exporter in vertebrate cells, cellular iron overload is susceptible to occur when iron homeostasis is disordered.[14] Iron is an important trace element involved in multiple biological processes such as DNA synthesis and energy production. However, the accumulation of unstable iron ions can lead to oxidative damage and cell death when cellular iron is overloaded.[13] Ferroptosis is a form of programmed cell death driven by iron-dependent lipid peroxidation, which has unique morphological, genetic, and biochemical characteristics.[17,18] Recent studies have reported ferroptosis in both in vivo and in vitro SMI models, and inhibition of ferroptosis by small molecule compounds has been found to be protective in SMI models.[19–21] Despite increased research focus on the role of ferroptosis in SMI, the current understanding of its molecular biology is still scattered and unclear, further in-depth exploration is necessary and urgent, which may lead to promising targets for diagnosis and treatment.

Deep transcriptomic analyses based on human pathological tissues contribute to bring the closest insights to reality in exploring the molecular biological mechanisms in various diseases, many of which have translated into clinical benefits.[22–25] However, current studies on the mechanisms of ferroptosis in SMI still lack important information from human heart samples. Here, we performed an in-depth analysis of the human septic heart transcriptomes, which identified the variations of ferroptosis-related genes (FRGs) in SMI, and further explored their potential biological functions and pathways. A protein-protein interaction (PPI) network was constructed to identify key functional modules and hub genes. The expression of hub genes and ferroptosis features was then validated in the mouse SMI model, and the diagnostic capability and prognostic relevance of key FRGs for SMI were subsequently evaluated. The expression and distribution of key FRGs were determined through human heart single-cell transcriptome data. Furthermore, we performed immune infiltration correlation analyses of identified key FRGs in septic hearts given the tight association between SMI, ferroptosis, and immune infiltration.[8,26–28] Finally, we predicted potential ferroptosis-modulating drugs for SMI based on the drug-target correlation of key FRGs, and performed molecular docking for further exploration.

Materials and Methods

Data Collection

As described in our previous study,[29] the microarray datasets GSE79962 and GSE54514 were retrieved from the GEO database (https://www.ncbi.nlm.nih.gov/geo/). The transcriptomic data of 11 control hearts (sourced from non-failed donors) and 20 septic hearts (sourced from patients who died from sepsis) were obtained from the GSE79962 dataset, while the transcriptomic data of whole blood samples (within 24 hours of admission to the intensive care unit) from 26 sepsis survivors and 9 sepsis nonsurvivors were obtained from the GSE54514 dataset. After probe merging and ID conversion, all expression data were log2 transformed and quantile normalized before further analyses.

Transcriptomic Differential Analysis and Identification of Differentially Expressed Genes (DEGs) and Differentially Expressed FRGs (DEFRGs)

The limma package (version 3.48.0) in the R software (version 4.1) was used to screen the DEGs in the septic hearts, and the Benjamini-Hochberg correction method was used to control the false-discovery rate (FDR). Referring to previous studies,[30,31] the thresholds we set for selecting the DEGs were FDR < 0.05 and $|\log2FC| \geq 0.25$. The FRGs were derived from the ferroptosis-related database FerrDB (version dated 10 May 2022) (http://www.zhounan.org/ferrdb/),[32] and the combined FRG set included a total of 388 FRGs after deduplication of genes (Table S1). DEGs and FRGs were overlap analyzed using the VennDiagram package in R software and the overlapped genes were defined as DEFRGs.

Gene Set Enrichment Analysis (GSEA)

To evaluate the overall correlation between FRGs and septic hearts, GSEA was performed using the Sangerbox online tool (http://vip.sangerbox.com/).[33] Genes in the ferroptosis-associated gene set obtained as mentioned above were scored and ranked by expression value in the GSE79962 dataset. Normalized enrichment score (NES) was calculated and FDR < 0.05 was considered significant.

Gene Ontology (GO) and Kyoto Encyclopedia of Genes and Genomes (KEGG) Enrichment Analyses

As described in our previous study,[29] the identified DEFRGs were subjected to GO and KEGG enrichment analyses using the clusterProfiler package in the R software.[34] FDR < 0.05 was the criterion for significantly enriched by DEFRGs.

PPI Network and Identification of Key Modules and Hub Genes

The STRING database (https://string-db.org/) and Cytoscape software were used to establish and visualize a PPI network of DEFRGs as described in our previous studies.[29] Functional key modules were identified from the PPI network by the MCODE plugin using the K-means clustering algorithm (degree cutoff = 2, node score cutoff = 0.2, K-core = 2). The genes in the PPI network were assigned and ranked accordingly by Cytohubba's built-in MCC algorithm, and the top ten genes were screened as hub genes.

Animals and Establishment of the SMI Model

Male BALB/c mice (8–10 weeks old) were adopted, provided by Charles River Laboratories. Mice were acclimatized for 1 week at 23±1°C under a 12 hours light/dark period, housed with bacteria-free water and food provided ad libitum. Twenty-one mice were used in the control group, while twenty-four mice per group were used in the experimental groups. To induce SMI, the mice were injected intraperitoneally with lipopolysaccharide (LPS, Sigma-Aldrich, USA) (10 mg/kg). The sham-operated controls received an equal volume of PBS. The LPS+Fer-1 group was pre-treated with Ferrostatin-1 (Fer-1, Sigma-Aldrich, USA) (5 mg/kg) 30 min before LPS injection. After 24 hours of LPS injection, mice received transthoracic echocardiography to identify the heart functions. The mice were then euthanized, and the blood and heart samples were collected for subsequent experiments. All animal experiments were approved by the Animal Experimentation Ethics Committee of the First Affiliated Hospital of Nanchang University (ethics number: CDYFY-IACUC-202209QR004), and all the laboratory procedures were followed the "Laboratory Animals-Guideline of welfare and ethics" of the State Standard of P.R. China for the welfare of animals.

Echocardiography

The mice were anesthetized with 1.5% isoflurane, and cardiac function was evaluated by two-dimensional transthoracic echocardiography using a Vevo2100 imaging system (VisualSonics, Canada). All measurements were performed by an experienced operator blinded to the study.

Biochemical Analyses

Blood samples were collected from the abdominal aorta. Serum levels of lactate dehydrogenase (LDH), creatine kinase-myoglobin binding (CK-MB), cardiac troponin T (cTnT), interleukin (IL)-6, IL-1β and tumor necrosis factor (TNF)-α were measured using specific ELISA kits (Nanjing Jiancheng Bioengineering Institute, China) according to the manufacturer's instructions. In addition, freshly collected myocardia (with removal of atriums) were homogenized in cold, the malondialdehyde (MDA), superoxide dismutase (SOD), glutathione peroxidase (GSH-Px), and reduced (GSH)/oxidized (GSSG) glutathione (GSH/GSSG) ratios were measured using specific kits according to the manufacturer's instructions (Nanjing Jiancheng Bioengineering Institute, China). The absorbance was measured using a Spark® multimode microplate reader (Tecan, Switzerland).

Measurement of Cardiac Iron Content

The myocardia (with removal of atriums) were weighed, homogenized and lysed. The iron content in the myocardium was measured using a kit according to the manufacturer's instructions (Pulilai Gene Technology, China). The absorbance was measured at 550 nm using the Spark® multimode microplate reader (Tecan, Switzerland).

Histological Analysis

Isolated hearts were fixed in 10% formalin, dehydrated and paraffin-embedded, and cut into 5-μm cross-axis sections. Hematoxylin and eosin (H&E) staining was performed according to the standard protocols. For immunohistochemical staining, the sections were sequentially probed with the anti-4 hydroxynonenal antibody (4-HNE, 1:200, Bioss, China), biotin-labeled goat anti-rabbit IgG antibody (1:100, Beyotime, China) and HRP-labeled Streptavidin (1:300, Beyotime, China), then HRP was detected by DAB kit (Beyotime, China).

Detection of Radical Oxygen Species (ROS)

Fresh isolated hearts were frozen sectioned after OCT embedding. The sections were incubated with a dihydroethidium (DHE) probe (Yeasen, China) at 37°C for 60 min away from light, and imaged under a fluorescence microscope (Nikon Eclipse Ci, Japan) fitted with a digital camera (Nikon DS-U3, Japan).

Transmission Electron Microscopy (TEM) Imaging

Fresh mice left ventricular myocardium (1 mm × 1 mm × 1 mm) were rapidly harvested. After fixation, washing, dehydration, embedding, sectioning and staining. The ultrastructure of myocardial mitochondria was observed by TEM (Hitachi 7800, Japan), and the Flameng score method was used to evaluate the ultrastructural damage of mitochondria.[35]

Western Blot Analysis

Western blotting was performed as described in our previous study.[29] Briefly, the myocardium (with removal of atriums) was homogenized and lysed, and the extracted proteins were separated by 10% sodium dodecyl sulfate-polyacrylamide gel electrophoresis (SDS-PAGE) and transferred to PVDF membranes. After blocking with 5% non-fat dry milk at room temperature for 2 hours, the blots were incubated overnight with primary antibodies against PTGS2 (Proteintech #12375-1-AP, China, 1:1000) and β-actin (Biosharp #BL005B, China, 1:2000) at 4°C. Subsequently, the membrane was incubated with the secondary antibody (Beyotime # A0208, China, 1:2000) for 2 hours at room temperature. The positive bands were visualized using the Ultra High Sensitivity ECL kit (Beyotime, China) and imaged using FluorChem FC3 (ProteinSimple, USA). The blots were densitometrically scanned using the ImageJ software (NIH, USA), and β-actin was selected as the internal reference according to previous studies.[36,37]

Quantitative Real-Time PCR (qRT-PCR)

The protocol for qRT-PCR has been described in our previous study.[29] Briefly, myocardia (with removal of atriums) were homogenized in TRIzol (Invitrogen, USA) to extract total RNA. After removal of genomic DNA by DNase treatment, total RNA was then reverse-transcribed into cDNA using RevertAid MM (ThermoFisher Scientific, USA) according to the manufacturer's instruction. qRT-PCR was performed using the Power SYBR Green PCR Master Mix (ThermoFisher Scientific, USA) on the real-time PCR system (StepOnePlus Real-Time PCR System, Applied Biosystems, USA). According to previous studies,[38,39] for normalization, ACTB levels were used as an internal reference and mRNA levels relative to control were calculated according to the $2^{-\Delta\Delta CT}$ method. The primers were designed using NCBI Primer-Blast and synthesized by Sangon Biotech Co. Ltd. (Shanghai, China), the sequences are listed in Table S2.

Receiver Operating Characteristic (ROC) Curve Analyses

To evaluate the diagnostic accuracy of genes, ROC curves were plotted as described in our previous study.[29] The area under the ROC curve (AUC) was used to quantify the classification. Genes with AUC > 0.6 were considered diagnostic, and those with AUC > 0.8 were considered excellently diagnostic.

Single-Cell Sequencing Analyses

The Single Cell Portal (https://singlecell.broadinstitute.org/single_cell) was availed to obtain single cell sequencing data for key FRGs. The single-cell sequencing data of the human fetal heart and adult heart from SCP498 and SCP1021 were used.[40,41]

Immune Infiltration Analyses

The Sangerbox platform (http://vip.sangerbox.com/) was used to perform immune infiltration analyses as previously described.[29] The proportion of 22 immune cell species was calculated using the CIBERSORT algorithm based on normalized gene expression data.

Potential Therapeutic Drug Prediction and Molecular Docking

The potential ferroptosis-regulating drugs for SMI were predicted by the Enrichr online enrichment analysis tool (http://amp.pharm.mssm.edu/Enrichr) based on the protein-drug interaction data from the DSigDB database (http://dsigdb.tanlab.org/).[42,43] The corresponding FDR and the combined score were calculated as described in the study of Avi Ma'ayan et al.[43] FDR < 0.05 and combined score > 10,000 were set as cut-offs for valid drug candidates, while higher combined scores were considered to have a stronger interaction between the drug and target genes.

Molecular docking was used to model the combination between drug and target proteins, and to predict the extent of the interaction. The chemical structures of the predicted drugs and target proteins were obtained from the PubChem database (http://pubchem.ncbi.nlm.nih.gov),[44] the RCSB protein data bank database (https://www.rcsb.org),[45] and the AlphaFold protein structure database (https://alphafold.ebi.ac.uk/).[46] After collating the receptor protein and ligand small molecule compounds separately, molecular docking was performed using the CDOCK module in Discovery Studio 2019 software (BIOVIA, USA).

Statistical Analyses

All the statistical analyses not mentioned above were performed using the Sangerbox platform and the GraphPad Prism (version 8.0.2, La Jolla, CA). Comparisons between two groups in the transcriptomic analyses which not mentioned above were performed using signed-rank test. Ordinary one-way ANOVA was used for comparisons between multiple groups in the animal experiments. The Spearman correlation test was used for correlation analysis. Data are presented in mean ± SD. The Benjamini-Hochberg correction method was applied to adjust the *P* values for FDR, and statistical significance was considered at FDR < 0.05. P values are shown as indicated: *P < 0.05, **P < 0.01, ***P < 0.001, ****P < 0.0001, ns = not significant.

Results

Overall Study Protocol

The illustrative and detailed protocol of our study is summarized (Figure 1A and B). All the raw data were normalized before further analyses, as shown in Figure S1.

Widespread Dysregulation of FRGs in the Human Septic Heart Transcriptomes

GSEA is a commonly utilized method to evaluate the overall relevance of specific characteristic gene set in the disease transcriptome to the disease phenotype.[22] To evaluate whether the variation of the FRG set in the human septic heart transcriptome is significant, the GSEA of total FRG set in the GSE79962 dataset was performed. The result of GSEA showed that FRGs were dramatically differentially expressed in the two groups, and the FRG set showed significant positive correlation with the septic heart phenotype compared to the control (FDR < 0.05, NES = 1.489) (Figure S2). This

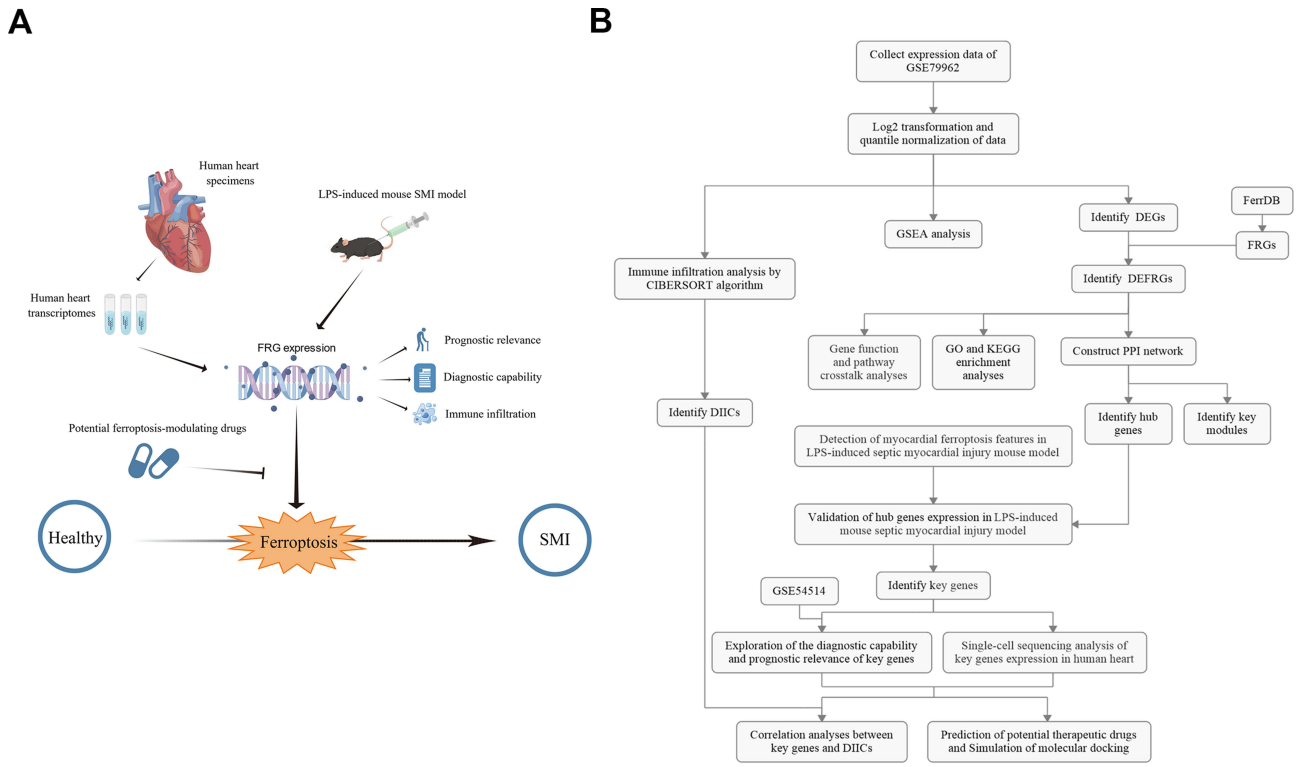

Figure 1 The overall protocol of this study. The illustrative (**A**) and detailed (**B**) protocol of this study, drawn by Figdraw.
Abbreviations: GSEA, Gene set enrichment analysis; DEG, differentially expressed genes; FRG, ferroptosis-related gene; DEFRG, differentially expressed FRG; GO, gene ontology; KEGG, Kyoto Encyclopedia of Genes and Genomes; PPI, protein-protein interaction; DIIC, differentially infiltrating immune cell; LPS, lipopolysaccharide.

result suggests that the widespread dysregulation of FRGs is present in the human septic heart transcriptomes as an essential feature, which indicates a functional correlation between ferroptosis and SMI.

Identification of DEGs and DEFRGs

There were significant transcriptomic differences between control and septic hearts, as shown in the clustered heatmap of genes in the top and last 250 of the log2FC ranking (Figure S3). There were 2316 DEGs identified from the GSE79962 dataset, as listed in Table S3, of which 1031 were upregulated and 1285 were downregulated in the septic hearts (Figure 2A).

Furthermore, we identified DEFRGs in the GSE79962 dataset since the GSEA result showed a meaningful association between the FRG set and septic heart phenotype. 71 out of the 388 FRGs obtained from FerrDB overlapped with the DEGs, which were identified as DEFRGs for subsequent analyses (Figure 2B), as listed in Table S4. These 71 DEFRGs were significantly differentially expressed in control and septic hearts, as shown in the clustered heatmap (Figure 2C). Further analysis of expression correlations between DEFRGs in septic hearts revealed numerous significant correlations, as shown in the correlation heatmap (Figure 2D). For example, *HIF1A* was significantly positively correlated with SAT1 ($r = 0.87$), and POR was significantly positively correlated with ELOVL5 ($r = 0.84$) and negatively correlated with NR1D2 ($r = -0.86$) and TSC1 ($r = -0.82$). These extensive correlations between genes suggest that intricate functional networks may exist in DEFRGs.

GO and KEGG Enrichment Analyses

To explore the functions and related pathways of the DEFRGs, we performed GO and KEGG enrichment analyses. The GO enrichment analyses showed that the DEFRGs are mainly involved in the biological processes (BP) of cellular iron ion homeostasis and response to nutrient, oxygen, and chemical stress (Figure 3A). Furthermore, cellular components (CC) to which the DEFRGs localize include apical part, basal plasma membrane, autophagosome or autolysosome

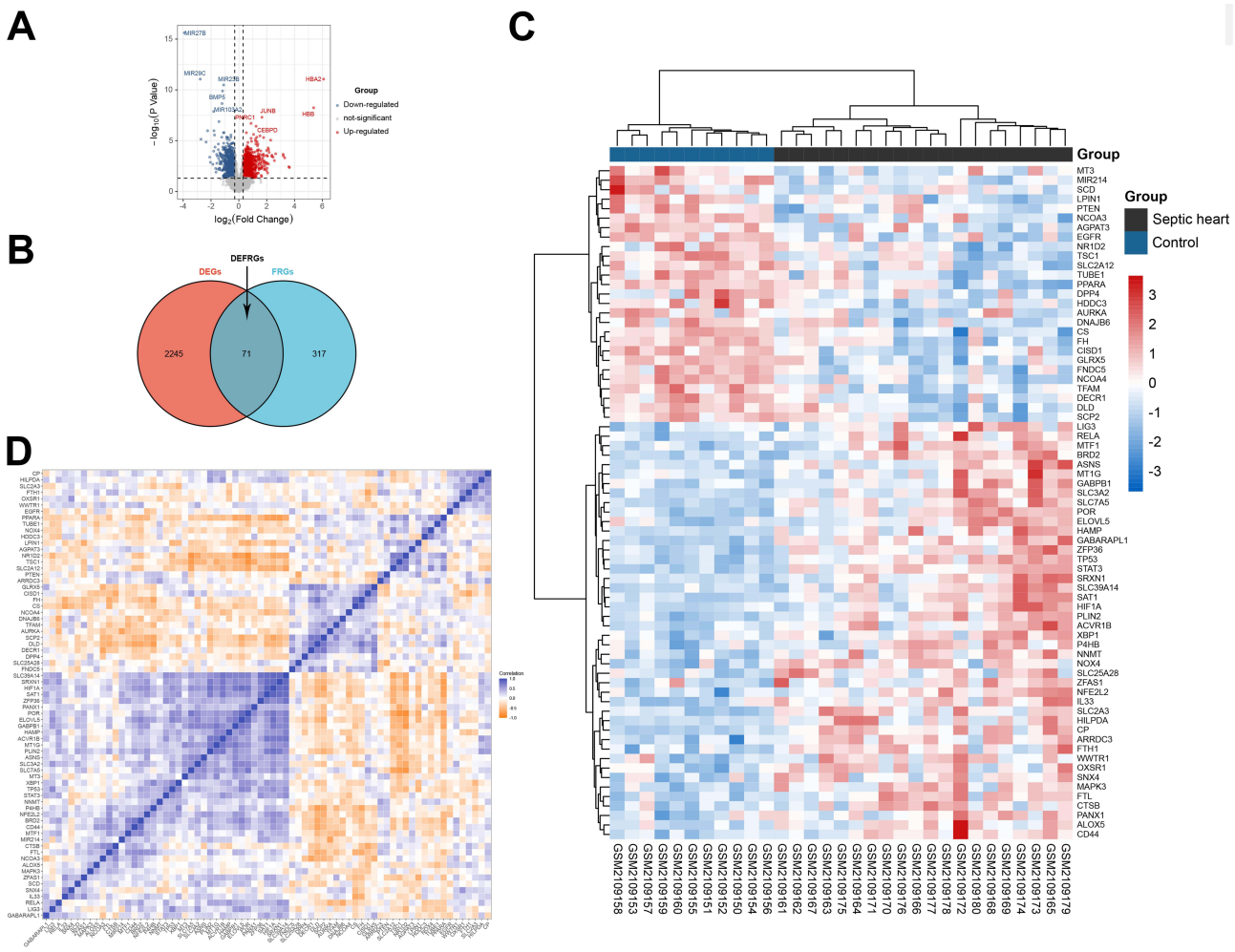

Figure 2 Identification of differentially expressed ferroptosis-related genes. Volcano plot of DEGs in the GSE79962 dataset (FDR < 0.05 and |log2FC| ≥ 0.25). (**B**) Venn diagram showing the overlap of genes between DEGs in the GSE79962 dataset and FRGs from FerrDB. (**C**) Clustered heatmap of DEFRGs in the GSE79962 dataset. (**D**) Correlation heatmap of DEFRGs in the septic hearts from the GSE79962 dataset. $N_{control}$ = 11, $N_{septic\ heart}$ = 20.

(Figure 3B). Among the molecular functions (MF), the DEFRGs were associated with the binding of DNA-binding transcription factor, ubiquitin protein ligase, transcription coregulator and coactivator, heat shock protein and the activities of acyltransferase and oxidoreductase (Figure 3C). The KEGG enrichment analysis showed that the DEFRGs are mostly involved in ferroptosis, reactive oxygen species, autophagy, and cancer-related pathways (Figure 3D). The cross-talks between gene functions and pathways were further analyzed, as shown in Figure 3E–H. DEFRGs have an intricate web-like relationship with different BP, CC, MF, and KEGG pathways, and the results suggested that FRGs regulate the progression of SMI may via the cross-talks of multiple gene functions and pathways rather than individually.

Construction of PPI Network and Identification of Key Modules and Hub Genes

Given the cross-talk of multiple genes and pathways in FRGs-mediated regulation of SMI, we subsequently constructed a PPI network of DEFRGs using the STRING database to identify functional gene clusters and individual genes among DEFRGs (Figure 4A). Two key modules (Figure 4B) and ten hub genes (*STAT3, NOX4, TP53, HIF1A, NFE2L2, MAPK3, RELA, PTEN, EGFR, PPARA*) (Figure 4C) were identified. Notably, the identified hub genes were exactly overlapped with one of the key modules, which further demonstrates the important pivotal role of these genes as major functional clusters in DEFRGs. Figure 4D and E show the multiple correlations between hub genes and with other DEFRGs.

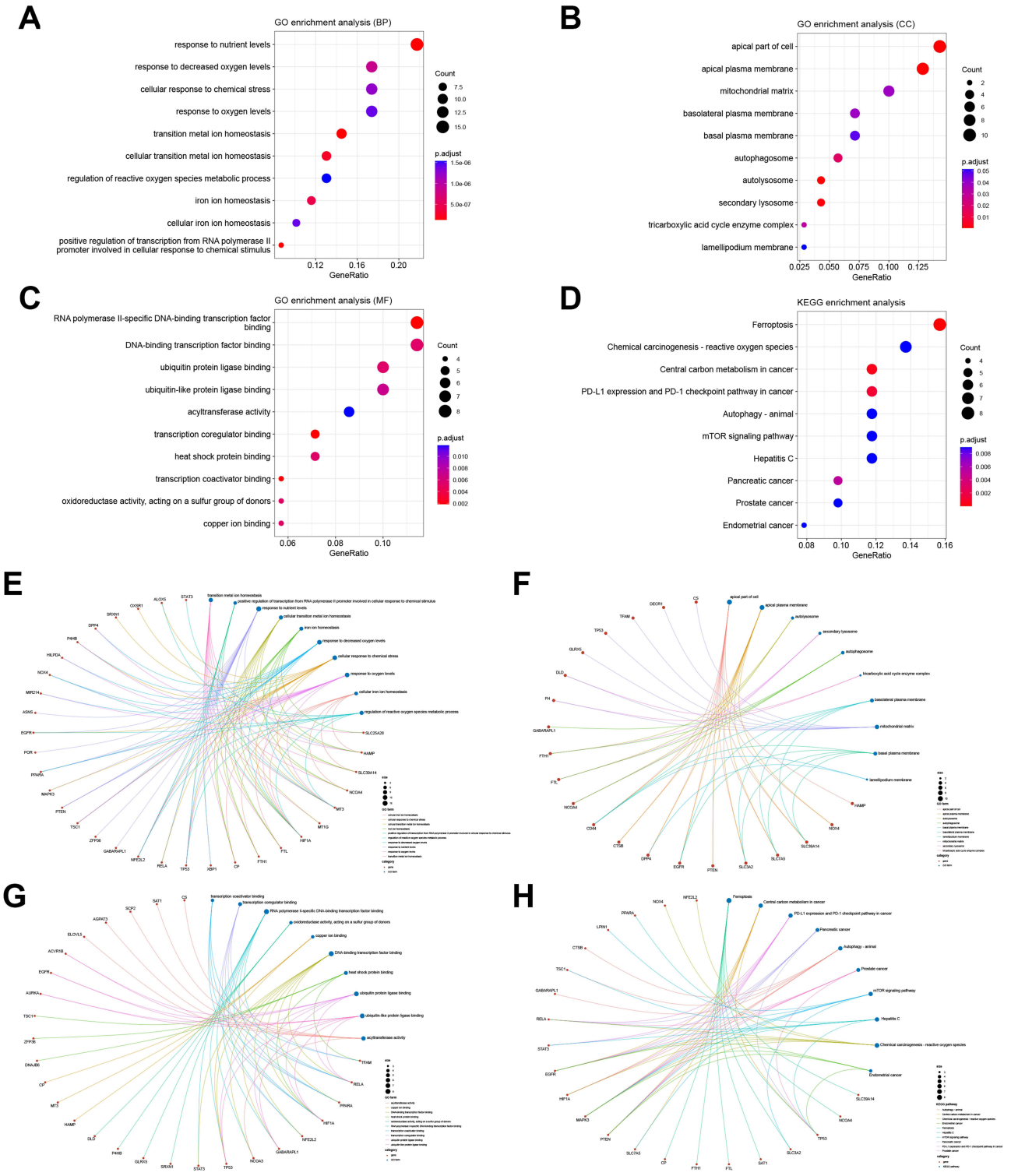

Figure 3 GO and KEGG enrichment analyses of differentially expressed ferroptosis-related genes. GO enrichment analyses of DEFRGs in (**A**) the biological process category (BP); (**B**) the cellular component category (CC); (**C**) the molecular function category (MF). (**D**) KEGG enrichment analysis of DEFRGs. Crosstalk analysis between DEFRGs and (**E**) gene functions in BP; (**F**) gene functions in CC; (**G**) gene functions in MF; (**H**) KEGG pathways.

Ferroptosis Features in LPS-Induced Mouse Septic Myocardial Injury Model

The LPS-induced mouse SMI model is a commonly used experimental model for exploring SMI in vivo, which we used here to observe the ferroptosis features and hub gene expression in SMI myocardium.[19,21,47] Cardiac dysfunction in the SMI mice was manifested by reduced left ventricular ejection fraction and fractional shortening (Figure 5A–C), along

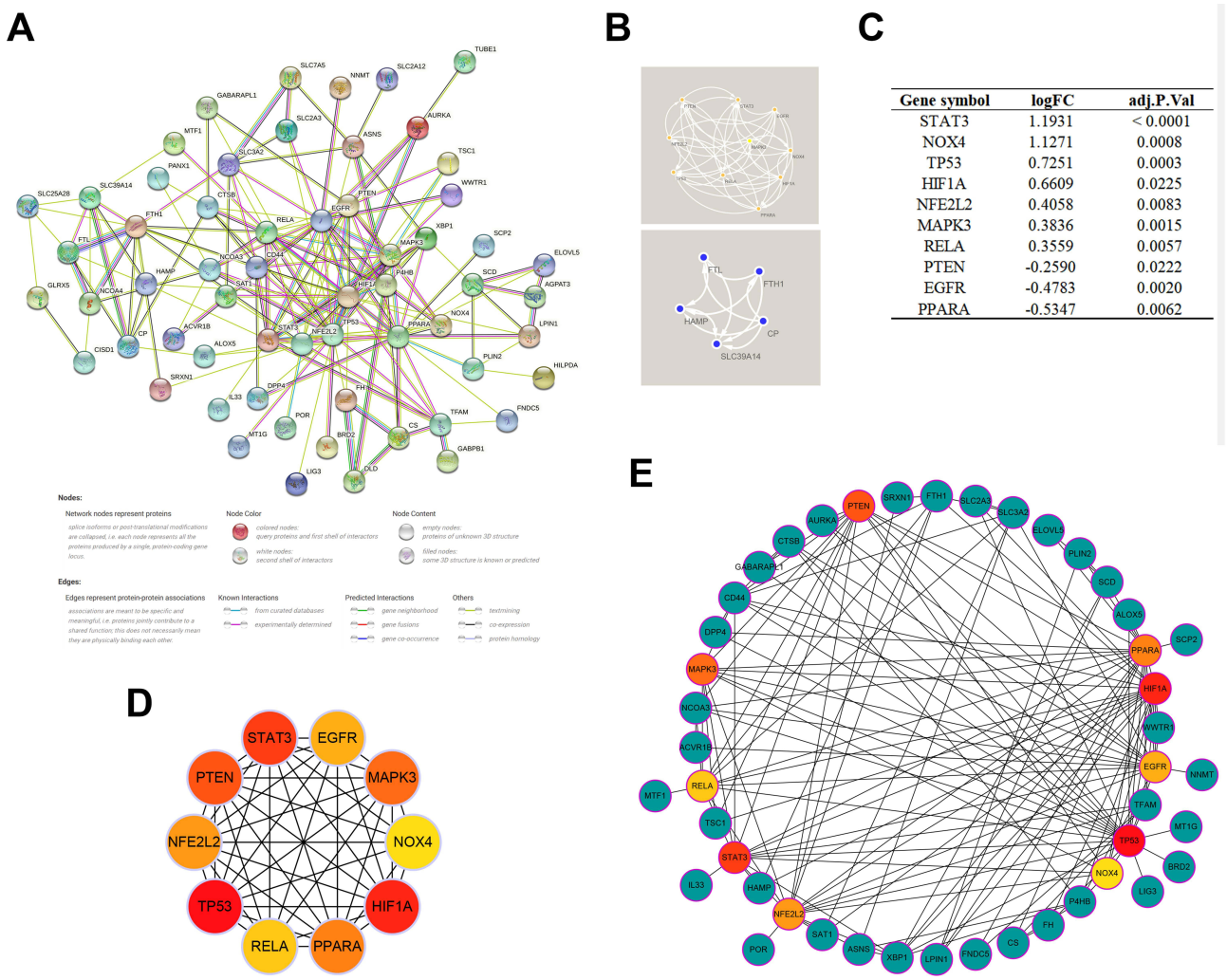

Gene symbol	logFC	adj.P.Val
STAT3	1.1931	< 0.0001
NOX4	1.1271	0.0008
TP53	0.7251	0.0003
HIF1A	0.6609	0.0225
NFE2L2	0.4058	0.0083
MAPK3	0.3836	0.0015
RELA	0.3559	0.0057
PTEN	-0.2590	0.0222
EGFR	-0.4783	0.0020
PPARA	-0.5347	0.0062

Figure 4 PPI network and identification of hub genes. (**A**) PPI network of all DEFRGs constructed by STRING database, the no connected dots were hidden. (**B**) Modules identified by the MCODE plugin using the K-means clustering algorithm (degree cutoff = 2, node score cutoff = 0.2, K-core = 2). (**C**) The expression variations of hub genes ranked by MCC algorithm in the septic hearts from the GSE79962 dataset. (**D**) Cross-talks between hub genes, the deeper color of the dot means that the rank order of the hub gene is more advanced. (**E**) Cross-talks between hub genes and other DEFRGs.

with increased serum inflammatory factors (IL6, IL-1β, TNF-α) and myocardial injury markers (LDH, CK-MB, cTnT), which could be partially rescued by the ferroptosis inhibitor Fer-1 (Figure 5D–I). The ferroptosis marker PTGS2 was upregulated in the myocardium of SMI mice at both mRNA and protein levels (Figure 5J–L). Consistent with this, the inflamed myocardial tissues of SMI mice exhibited the biochemical and morphological features of ferroptosis, such as high levels of ROS and 4-HNE, and extensive mitochondrial damage characterized by atrophy and matrix loss (Figure 5M and N). Furthermore, we also observed increased levels of iron and MDA, decreased levels of SOD and GSH-Px, and reduced GSH/GSSG ratio in the myocardia of SMI mice (Figure 5O–S). Fer-1 protected against most of these pathological alterations, although there was no significant decrease in cardiac iron content, most likely due to the fact that Fer-1 only chelates Fe^{2+} rather than expelling iron from cells.[48] These results suggest that ferroptosis is a crucial pathological driver of SMI, and targeting ferroptosis pathways can be a promising therapeutic strategy for SMI.

Identification of Key FRGs and Exploration of Their Diagnostic Capability and Prognostic Relevance

We sequentially validated the expression of hub genes in the myocardium of SMI mice. As shown in Figure 6A–J, most of these genes showed trends consistent with that in the human septic heart transcriptome, such as increased expression

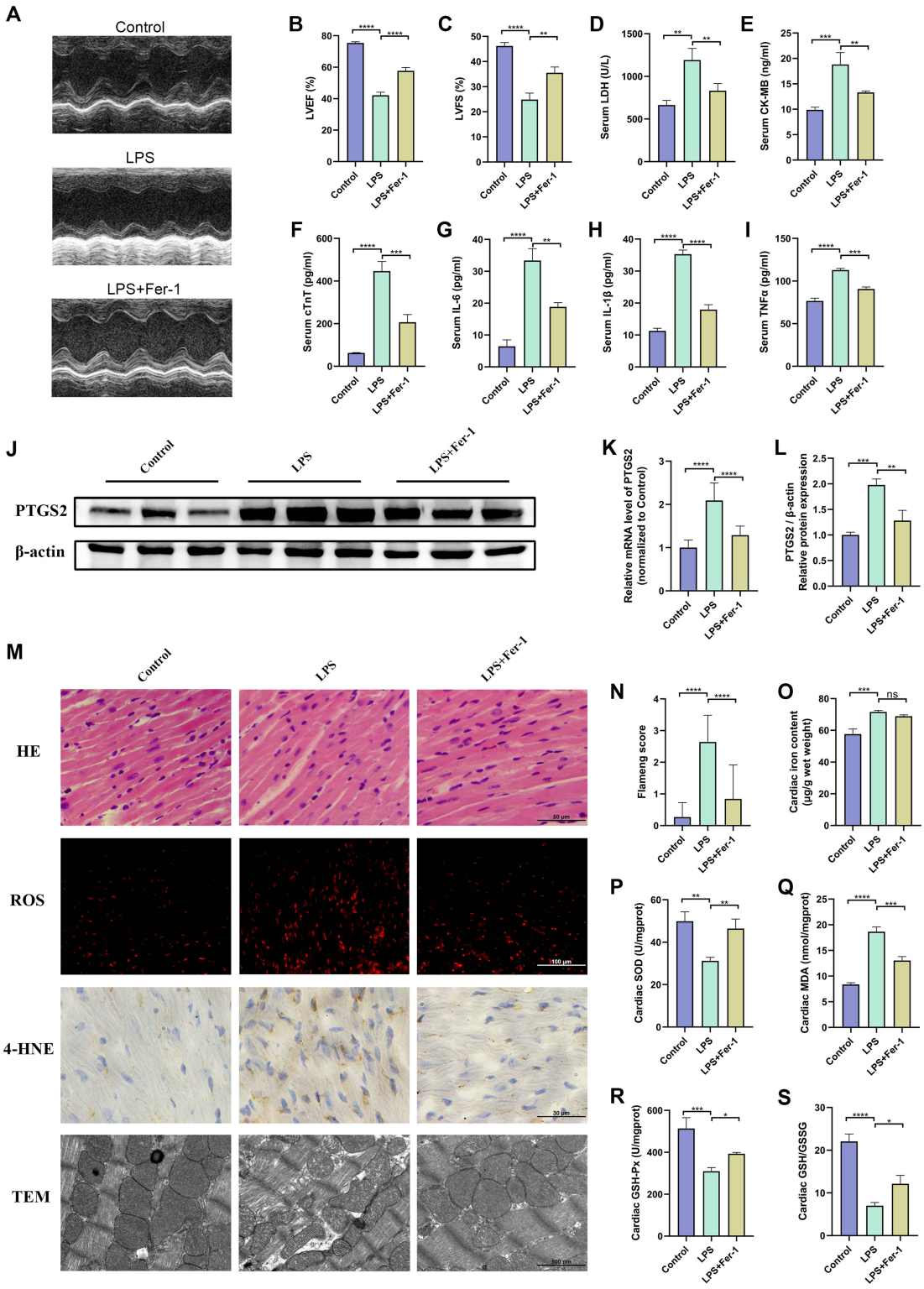

Figure 5 Altered ferroptosis features in LPS-induced mouse septic myocardial injury model. Male BALB/c mice (8–10 weeks old) were treated with LPS (10 mg/kg) for 24 hours in the presence or absence of Fer-1 (5 mg/kg) pretreatment, while the sham-operated controls received an equal volume of PBS, followed by subsequent experiments. Cardiac function evaluated by echocardiography in each group (**A**), quantified as (**B**) left ventricular ejection fraction (LVEF), (**C**) left ventricular fractional shortening (LVFS%) (N = 3 per group). Serum levels of (**D**) LDH, (**E**) CK-MB, (**F**) cTnT, (**G**) IL-6, (**H**) IL-1β, (**I**) TNF-α in each group (N = 3 per group). (**J**) Representative Western blotting bands of PTGS2. Quantification of (**K**) mRNA and (**L**) protein expression levels of PTGS2 in the left ventricular myocardium in each group (N = 9 for mRNA and N = 3 for protein per group). (**M**) Representative images of HE, DHE (ROS detection), 4-HNE staining and transmission electron microscopy in the left ventricular myocardium in each group (N = 3 per group). (**N**) Ultrastructural damage evaluated with the Flameng score method in each group. Cardiac levels of (**O**) iron, (**P**) SOD, (**Q**) MDA, (**R**) GSH-Px and (**S**) GSH/GSSG ratios in each group (N = 3 per group). *P < 0.05, **P < 0.01, ***P < 0.001, ****P < 0.0001, Data are presented as the mean ± SD, n ≥ 3.

Abbreviations: ns, not significant.

of *HIF1A, MAPK3, NOX4, RELA, STAT3 and TP53*, and decreased expression *PPARA* and *PTEN*. The Fer-1 treatment could partially but not completely reverse these alterations, suggesting that these genes may participate in other biological processes alongside ferroptosis. Interestingly, the *EGFR* expression was similar in the myocardium of SMI and control mice, while *NFE2L2* even showed opposite expression trend, which may be attributed to the presence of individual differences or different biological circumstances, and we excluded them as key genes given these uncertain expression alterations.

We finally identified *HIF1A, MAPK3, NOX4, PPARA, PTEN, RELA, STAT3 and TP53* as key FRGs, and further ROC analyses revealed that all of them have excellent diagnostic capability for septic heart (AUC > 0.8) (Figure 6K–R). Furthermore, the expression of several key FRGs (*PPARA, HIF1A, MAPK3, RELA, TP53* and *STAT3*) was significantly lower in the whole blood of sepsis non-survivors on the first day of ICU admission compared to survivors, indicating their relevance to the prognosis of sepsis (Figure 6S), further analysis revealed that *PPARA* and *TP53* expression in whole blood of sepsis patients was significantly negatively correlated with APACHEII scores-quantified severity (Figure 6T and U, S4). Interestingly, while SMI in general usually leads to poor prognosis in sepsis, we found the variability trends of key FRGs in the septic hearts do not fully coincide with those in whole blood of sepsis non-survivors, probably due to the comprehensive pathological condition of sepsis as a complex systemic disease. To conclude, these key genes that regulating ferroptosis in SMI have the potential to serve as biomarkers for SMI.

Distribution of Key FRGs in Human Heart

To explore the distribution of key FRGs in human heart, we investigated single-cell sequencing of key FRG expression using the Single Cell Portal. All key FRGs were expressed to varying degrees in both human fetal and adult hearts (Figure 7A and B). Noticeably, while key FRGs are predominantly expressed in cardiomyocytes, they are also expressed in other cell types such as immune cells.

Immune Infiltration Analyses

Immune cells play an important role in many cardiac diseases.[49,50] The immune and inflammatory responses are critical to the pathological progression of SMI.[8,51] Since single-cell sequencing analysis revealed that the key FRGs are also expressed in immune cells, while a close association between ferroptosis and immune cell function and activity has been reported in other biological environments, the immune infiltration analyses were further performed in our study to explore the cross-talks between ferroptosis and immune cells in SMI.[28,52,53] We estimated the relative proportions of infiltrating immune cells in each heart sample from the GSE79962 dataset using the CIBERSORT algorithm, as shown in Figure 8A, while the clustered heatmap of infiltrating immune cells shows the differences between control and septic hearts (Figure 8B). M2 macrophage was found at the highest proportion among immune cells in these heart samples, and it was lower in septic hearts (0.35 ± 0.08 vs 0.37 ± 0.08, septic hearts vs control), corresponding to a higher proportion of M1 macrophage (0.02 ± 0.04 vs 0.005 ± 0.01, septic hearts vs control) However, M1 and M2 macrophage did not show significance due to large individual differences ($p > 0.05$). The proportion of infiltrating neutrophils and resting NK cells was significantly increased in the septic hearts, while that of resting mast cells and $CD8^+$ T cells were significantly decreased, which were identified as differentially infiltrating immune cells (DIICs) in the SMI myocardium (Figure 8C).

Further analyses revealed correlations between immune cells (Figure S5A) and with several key FRGs in the septic hearts (Figure 8D), the proportion of resting mast cells was significantly positive correlated with *PPARA* expression and significantly negative correlated with *HIF1A* expression, and the proportion of neutrophils was significantly negative correlated with *TP53, HIF1A*, and *STAT3* expression, while that of resting NK cells was significantly positive correlated with *PTEN* and *RELA* expression (Figure S5B). In contrast, none of these correlations were significant in control hearts, suggesting that the correlation between key FRGs and immune cells may be pathological rather than physiologically present.

Potential Therapeutic Drug Prediction and Molecular Docking

We screened for potential drug candidates for SMI based on the key FRGs using the DSigDB database, which may treat SMI by modulating ferroptosis. Finally, 13 potential therapeutic drugs were predicted, as listed in Table S5. Figure 9A

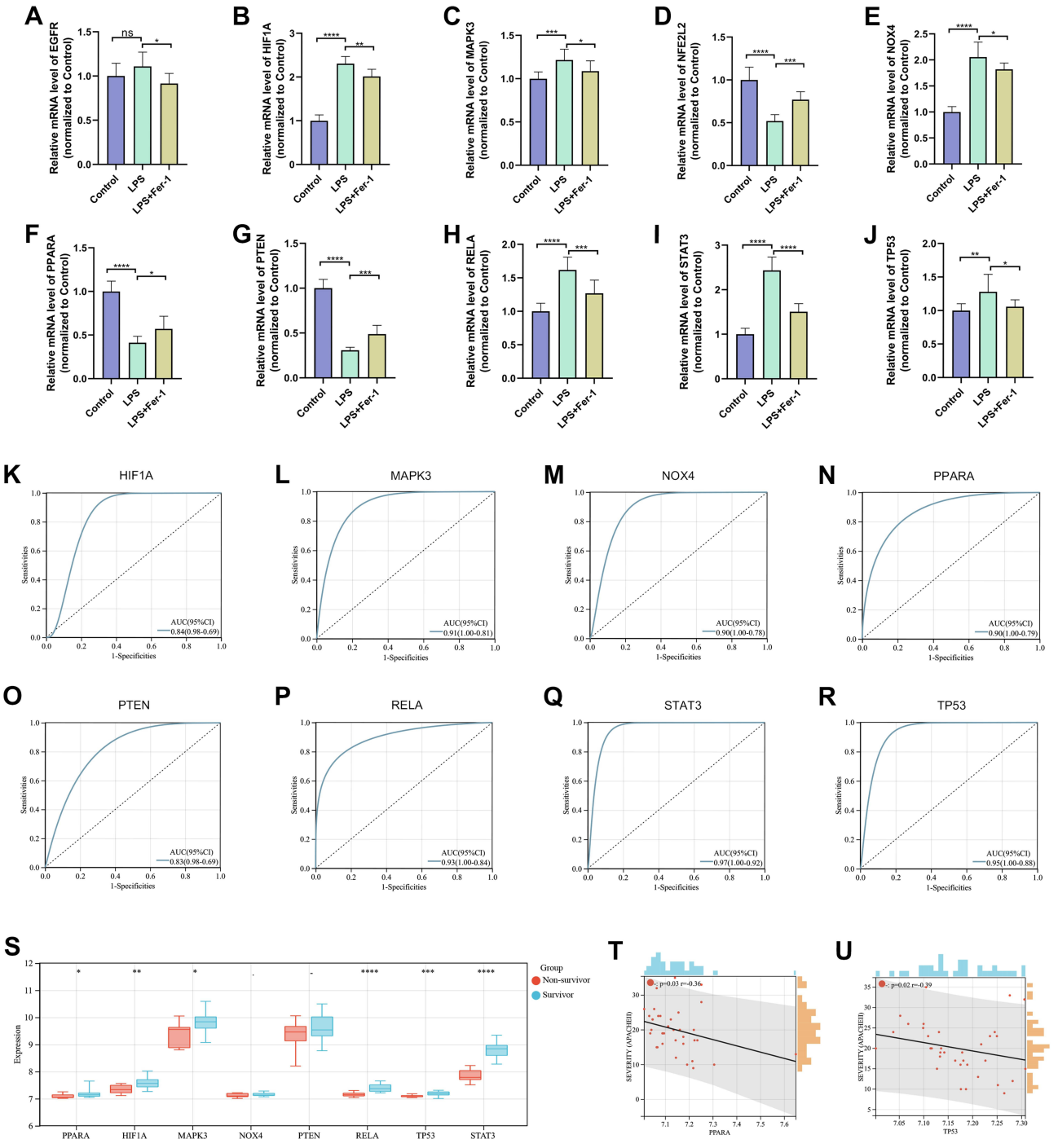

Figure 6 Identification of key FRGs and exploration of their diagnostic capability and prognostic relevance. mRNA expression levels of (**A**) EGFR, (**B**) HIF1A, (**C**) MAPK3, (**D**) NFE2L2, (**E**) NOX4, (**F**)PPARA, (**G**) PTEN, (**H**) RELA, (**I**) STAT3, (**J**) TP53 in each group detected by qRT-PCR (N = 9 per group). ROC curves show the diagnostic capability of (**K**) HIF1A, (**L**) MAPK3, (**M**) NOX4, (**N**) PPARA, (**O**) PTEN, (**P**)RELA, (**Q**) STAT3, (**R**) TP53 for SMI in hearts from the GSE79962 dataset, $N_{control}$ = 11, $N_{septic\ heart}$ = 20. (**S**) Comparison of key FRG expression in whole blood from sepsis survivors and nonsurvivors in GSE54514, $N_{survivor}$ = 26, $N_{Non\text{-}survivor}$ = 9. Linear regression plots presenting the significant correlation of APACHE II score-quantified severity with PPARA (**T**) and TP53 (**U**) expression in whole blood from GSE54514, N = 35. *P < 0.05, **P < 0.01, ***P < 0.001, ****P < 0.0001. Data are presented as the mean ± SD.

Abbreviations: ns, not significant.

shows the top ten predicted potential therapeutic drugs ranked according to the combined score, and resveratrol ($C_{14}H_{12}O_3$) was the most strongly drug-target correlated drug predicted for ferroptosis-related key genes (Combined Score = 2975802) (Figure 9B). Further molecular docking simulations showed that resveratrol formed stable complexes

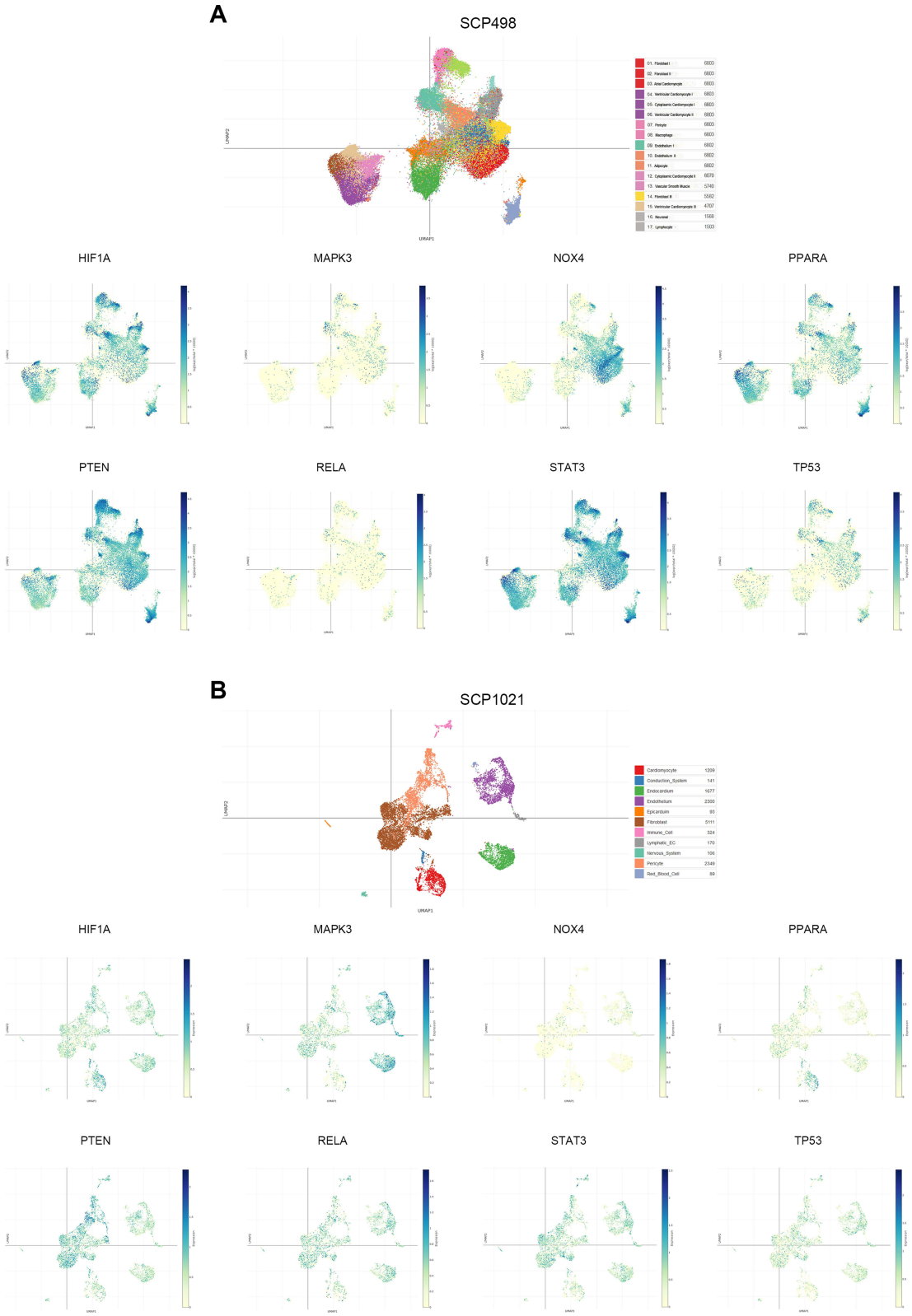

Figure 7 Distribution of key FRGs in human heart. Expression distributions of all key FRGs in single-cell sequencing data from (**A**) human adult hearts derived from SCP498 and (**B**) human fetal hearts derived from SCP1021.

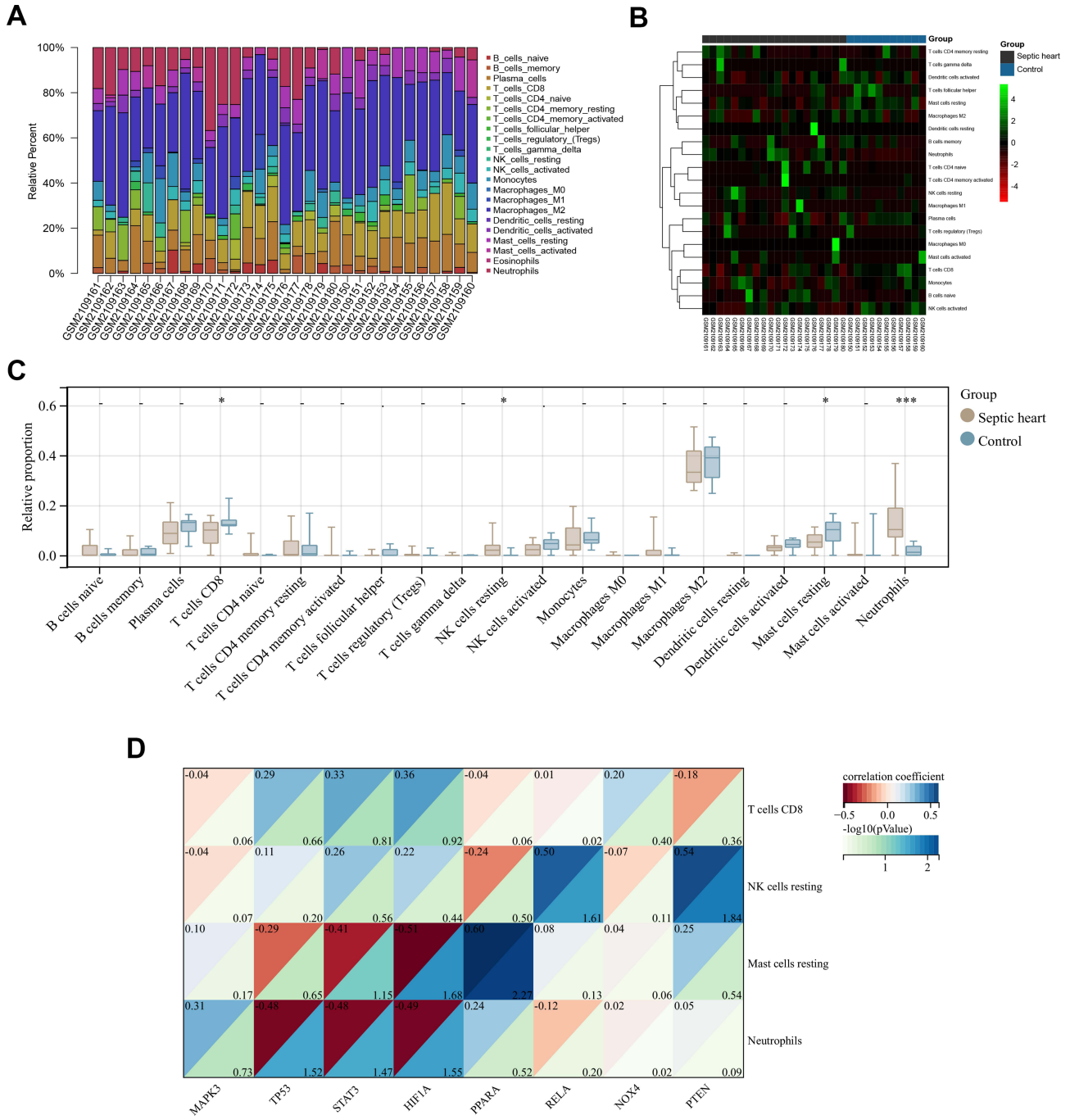

Figure 8 Correlation analyses between the proportion of DIICs and the expression of key FRGs. (**A**) The proportion of infiltrating immune cells estimated by the CIBERSORT algorithm on hearts from the GSE79962 dataset. (**B**) Clustered heatmap of the proportion of DIICs in the GSE79962 dataset (**C**) Comparison of infiltrating immune cells proportion between control and septic hearts in the GSE79962 dataset, immune cell with zero proportion was hidden. (**D**) Correlation heatmap of DIICs proportion with key FRGs expression in the septic hearts from the GSE79962 dataset. $N_{control}$ = 11, $N_{septic\ heart}$ = 20. *P < 0.05, ***P < 0.001.

with all key FRGs (Figure 9C), especially PTEN (-CDOCKER Interaction Energy = 38.57) and RELA (-CDOCKER interaction energy = 33.56), as shown in Figure 9D.

Discussion

Given the diagnostic uncertainty and serious prognostic impact of SMI, it is crucial to elucidate the underlying pathophysiological mechanisms, and identify reliable diagnostic markers and therapeutic targets for clinical practice.

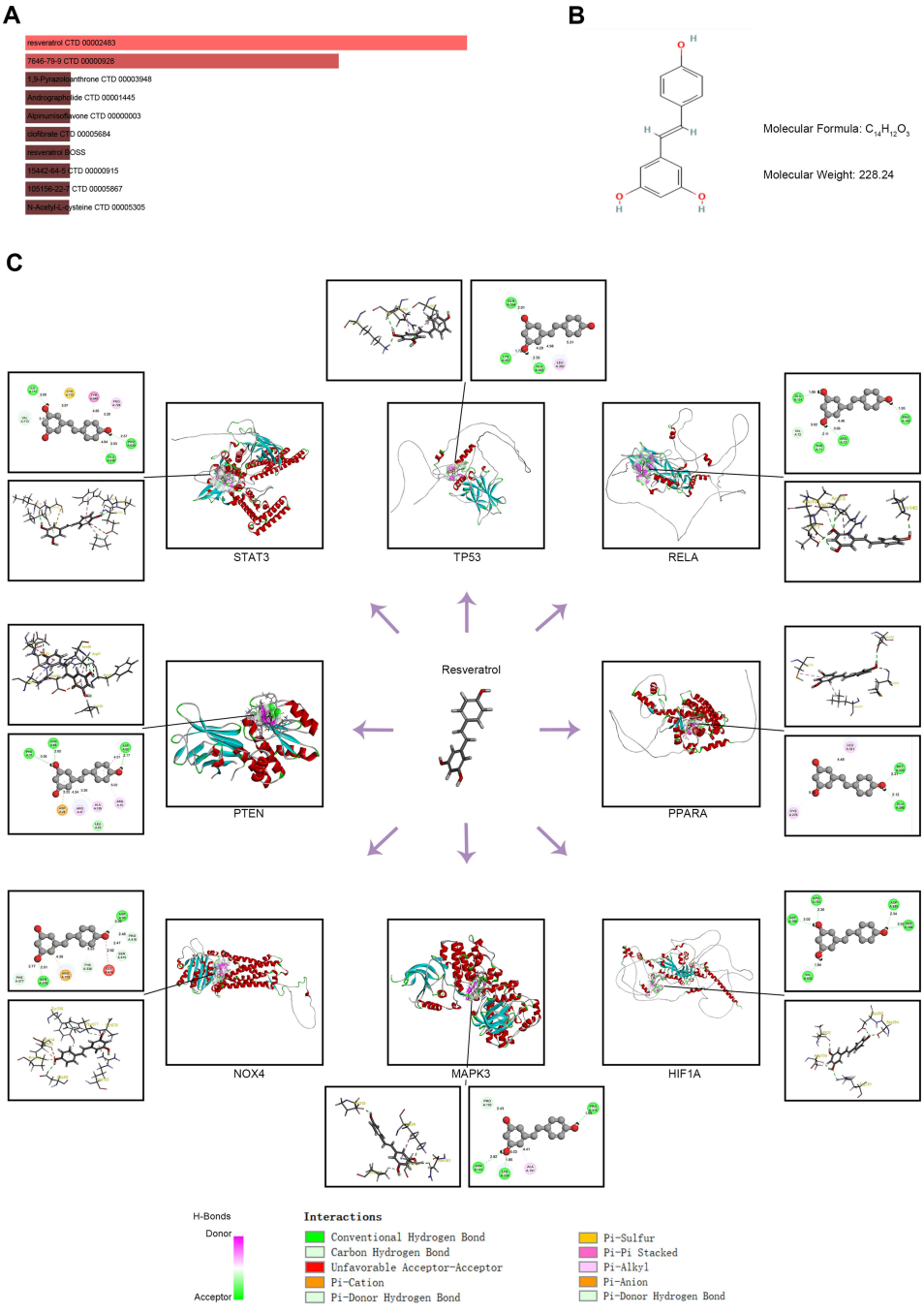

D

Name	Role	Sources of Structure	ID	-CDOCKER Energy	-CDOCKER Interaction Energy
Resveratrol	Ligand	Pubchem Datebase	PubChem ID 445154	-	-
PTEN	Receptor	RCSB Protein Data Bank Database	PDB ID 7JVX	28.376	38.574
RELA	Receptor	AlphaFold Protein Structure Database	UniProt ID Q04206	24.8787	33.5562
PPARA	Receptor	AlphaFold Protein Structure Database	UniProt ID Q07869	23.2919	32.397
MAPK3	Receptor	RCSB Protein Data Bank Database	PDB ID 4QTB	22.8397	31.8021
NOX4	Receptor	AlphaFold Protein Structure Database	UniProt ID Q9NPH5	22.3946	30.7867
STAT3	Receptor	AlphaFold Protein Structure Database	UniProt ID P40763	20.4522	29.2877
TP53	Receptor	AlphaFold Protein Structure Database	UniProt ID P04637	16.5733	26.1603
HIF1A	Receptor	AlphaFold Protein Structure Database	UniProt ID Q16665	13.452	22.1553

Figure 9 Potential therapeutic drug prediction and molecular docking. (**A**) The top ten potential therapeutic drugs ranked according to combined score in the DSigDB database. (**B**) The chemical structures of resveratrol. (**C**) Molecular docking simulations showed that resveratrol formed stable complexes with all key FRGs. (**D**) Detailed information on molecular docking simulations of resveratrol with all key FRGs.

Ferroptosis has recently been reported as a noteworthy pathological mechanism in SMI, however, the underlying functional and regulatory mechanisms still unclear. Rapid advances in transcriptomic studies have improved our understanding of disease. In this study, we comprehensively analyzed dysregulated FRGs in the human septic heart transcriptomes, including regulatory mechanisms, functional pathways, key genes and their diagnostic capacity, immune infiltration relevance and potential ferroptosis-targeting drugs, and further validated prognostic relevance and key gene expression through an independent cohort of sepsis patients and in vivo SMI model, which provides new insights to explore the role of ferroptosis in the development of SMI.

Widespread dysregulation of ferroptosis-related genes in the septic hearts was identified by GSEA, suggesting that ferroptosis is an essential pathological mechanism of SMI, which corroborates previous studies.[14,47,54] Further GO enrichment analyses revealed that the cellular component localization, molecular functions, and biological processes of dysregulated FRGs in SMI have mostly been demonstrated or observed to be associated with ferroptosis in different biological circumstances. Ferroptosis is a form of programmed cell death caused by iron-dependent lipid peroxidation and massive accumulation of ROS, and its cellular sensitivity was demonstrated to be controlled by a combination of energy metabolism, iron homeostasis and oxidative stress responses.[18,55] Lipid peroxidation of the plasma membrane is an essential part of the ferroptosis process, ferritinophagy is also being focused on as a regulatory process of intracellular iron metabolism and cascade response to ferroptosis.[18,56,57] Transcription factor regulation, protein ubiquitination, and regulation of oxidoreductase activity have been reported as key functions of many ferroptosis-regulating molecules that have a strong influence on the ferroptosis process.[58–60] Apart from ferroptosis and ROS-related pathways, the dysregulated FRGs in SMI were also enriched in some cancer-related pathways, suggesting that some key molecules and pathways that regulate ferroptosis in SMI may not yet be defined. We believe that these enrichment results and the cross-talks between them warrant further investigation to clarify the specific mechanisms that affecting and being affected by ferroptosis in SMI.

We identified eight key dysregulated FRGs in the septic hearts by constructing a PPI network, and validated them in an in vivo model of SMI. All key FRGs had convincing evidence to support their regulation of ferroptosis in different biological circumstances,[32] in which *NOX4, PTEN* and *MAPK3* are positive regulators,[61–63] while *PPARA* and *RELA* are negative regulators,[64,65] and *HIF1A, STAT3* and *TP53* were bidirectional regulators.[66–68] Interestingly, while septic hearts were generally in a ferroptosis-activated state, the expression of the positive regulator *PTEN* is significantly reduced while the expression of the negative regulator *RELA* is significantly increased. We consider that this may attribute to their hitherto unrecognized bidirectional regulatory effect on ferroptosis or their simultaneous involvement in biological processes independent of ferroptosis in SMI. *HIF1A* and *TP53* were identified in a previous study as key genes that regulate autophagy in SMI, and our enrichment analysis also found that dysregulated FRGs were enriched in the autophagy pathway, suggesting that autophagy and ferroptosis may be closely associated in SMI. Some key FRGs have been identified as essential targets in the development of SMI pathology, and regulation of ferroptosis may be their unidentified molecular biological function in SMI, yet further studies are required to elucidate the specific regulatory mechanisms.[69–73]

The relationship between immune cell infiltration and SMI is complex and poorly understood. Immune and inflammatory responses are a double-edged sword in the pathological development of SMI.[8,74,75] The correlations between ferroptosis and immune cells have been demonstrated.[53] While immune cells can influence cellular ferroptosis by regulating iron metabolism or releasing cytokines, ferroptosis can also regulate the proliferation, function, activation and death of immune cells. However, the correlation between ferroptosis and immune infiltration in SMI is of interest but remains unclear. M2 macrophage, as an important anti-inflammatory immune cell, was the most abundant immune cell in the heart samples we studied. Its important functionality and abundant proportion in the heart have been reported in previous studies,[76–78] but it did not show differences in the control and septic hearts we studied, suggesting that there may be individual differences in its role in SMI which require further research. The proportion of infiltrating neutrophils and resting NK cells were increased in the septic hearts we analyzed, while that of infiltrating resting mast cells and $CD8^+$ T cells was decreased, which has been partially observed in previous research.[79–82] Several significant correlations between key FRGs and infiltrating immune cells in the septic hearts were identified, which may be pathological cross-talks between ferroptosis and abnormal immune responses in SMI as these correlations were not present in the healthy

counterparts. Nevertheless, some immune cells can exhibit both proinflammatory and antiinflammatory biological functions, and hyper-inflammation may coexist with immunoparesis in SMI, immune infiltration in SMI also varies by individual and disease stage, thus further investigation of the relationship between ferroptosis and immune infiltration in SMI is required.[8,83,84]

There is considerable interest in exploring effective therapies for diseases based on essential pathobiological targets.[3,85] Here, we predicted potential ferroptosis-modulating drugs for SMI based on the key FRGs, and resveratrol in particular showed high drug-target relevance. Echoing our study, resveratrol has been shown to alleviate SMI through multiple mechanisms, such as enhancement of SERCA2a activity by promoting the phospholamban oligomerization,[86] activation of the PI3K/AKT/mTOR and Nrf2 pathways,[87,88] and inhibition of the NF-κB signaling pathway and iron transport from plasma to myocardium.[88,89] Ferroptosis has recently been identified as one of the mechanisms by which resveratrol alleviates SMI,[21] and our study provides the molecular basis and potential targets for further investigation of how resveratrol regulates ferroptosis in SMI.

Our study provides evidence and new insights into the dysregulation of FRGs in the human septic heart transcriptome to explore the role of ferroptosis in SMI. Nevertheless, some limitations ought to be considered. Although the occurrence of ferroptosis has been conclusively observed in various experimental models of SMI and targeting ferroptosis has shown a protective effect in alleviating SMI, most studies in human SMI hearts, including our study, have only identified the occurrence of ferroptosis in terms of biochemical indicators or biomarkers while the corresponding morphological features are lacking. The data on the immune cell proportions of heart samples were derived from the side evidence provided by the CIBERSORT algorithm, which may present bias. Several protein structures used for molecular docking were predicted based on available vestigial PDB structures, as complete experimentally observed protein structures were not yet available. In addition, the human septic heart transcriptomes we used for analyses may only be representative of terminal SMI patients or those with poor prognoses as derived from patients who died of sepsis. To identify more reliable diagnostic and therapeutic targets, and translate our findings to clinical benefit, further mechanistic and functional studies of the identified key FRGs to adequately understand their regulation of ferroptosis in SMI are needed.

Conclusion

We identified the widespread dysregulation of FRGs in the human septic heart transcriptomes, and further bioinformatic analysis showed that dysregulated FRGs are mainly localized to the apical part, basal plasma membrane, and autophagosome/autolysosome, and regulate iron ion homeostasis and response to nutrient, oxygen, and chemical stress by affecting the binding of DNA-binding transcription factors, ubiquitin protein ligase, transcription coregulator and coactivator, heat shock protein and the activities of acyltransferase and oxidoreductase. The ferroptosis features and expression of key FRGs (*HIF1A, MAPK3, NOX4, PPARA, PTEN, RELA, STAT3 and TP53*) were validated in an in vivo SMI model, and key FRGs showed excellent diagnostic capability, along with significant correlation with the prognosis and immune infiltration. Furthermore, we predicted resveratrol as a potential therapeutic drug by regulating ferroptosis in SMI. Our study provides human septic heart transcriptome-based evidence and new insights into the role of ferroptosis in SMI, which is significant for deepening the understanding of the pathobiological mechanisms of SMI and exploring diagnostic and therapeutic targets for SMI.

Data Sharing Statement

Publicly available datasets were utilized in this study. The data used to support the results of this study are available from the online website mentioned above, and further inquiries can be directed to the corresponding author.

Ethics Statement

All animal experiments were approved by the Animal Experimentation Ethics Committee of the First Affiliated Hospital of Nanchang University (ethics number: CDYFY-IACUC-202209QR004). GEO database is a publicly accessible database, and includes patient data that have obtained ethical approval. There are no other required ethical statements.

Author Contributions

All authors made a significant contribution to the work reported, whether that is in the conception, study design, execution, acquisition of data, analysis and interpretation, or in all these areas; took part in drafting, revising or critically reviewing the article; gave final approval of the version to be published; have agreed on the journal to which the article has been submitted; and agree to be accountable for all aspects of the work.

Funding

This research was supported by the National Natural Science Foundation of China (No. 81960059), the Natural Science Foundation of Jiangxi, China (No. 20212BAB206021, No. 20224ACB206002, No. 20192BAB205004) and Jiangxi Province College students innovation and entrepreneurship Training Program (S202110403016).

Disclosure

The authors report no conflicts of interest in this work.

References

1. Gotts JE, Matthay MA. Sepsis: pathophysiology and clinical management. *BMJ*. 2016;353:i1585. PMID: 27217054. doi:10.1136/bmj.i1585
2. Singer M, Deutschman CS, Seymour CW, et al. The third international consensus definitions for sepsis and septic shock (Sepsis-3). *JAMA*. 2016;315(8):801–810. PMID: 26903338. doi:10.1001/jama.2016.0287
3. Huang M, Cai S, Su J. The pathogenesis of sepsis and potential therapeutic targets. *Int J Mol Sci*. 2019;20(21). PMID: 31671729. doi:10.3390/ijms20215376
4. Perner A, Gordon AC, De Backer D, et al. Sepsis: frontiers in diagnosis, resuscitation and antibiotic therapy. *Intensive Care Med*. 2016;42(12):1958–1969. PMID: 27695884. doi:10.1007/s00134-016-4577-z
5. Prescott HC, Angus DC. Enhancing Recovery From Sepsis: a Review. *JAMA*. 2018;319(1):62–75. PMID: 29297082. doi:10.1001/jama.2017.17687
6. Martin L, Derwall M, Al Zoubi S, et al. The septic heart: current understanding of molecular mechanisms and clinical implications. *Chest*. 2019;155(2):427–437. PMID: 30171861. doi:10.1016/j.chest.2018.08.1037
7. Walley KR. Sepsis-induced myocardial dysfunction. *Curr Opin Crit Care*. 2018;24(4):292–299. PMID: 29846206. doi:10.1097/mcc.0000000000000507
8. Hollenberg SM, Singer M. Pathophysiology of sepsis-induced cardiomyopathy. *Nat Rev Cardiol*. 2021;18(6):424–434. PMID: 33473203. doi:10.1038/s41569-020-00492-2
9. Lin Y, Xu Y, Zhang Z. Sepsis-induced myocardial dysfunction (SIMD): the pathophysiological mechanisms and therapeutic strategies targeting mitochondria. *Inflammation*. 2020;43(4):1184–1200. PMID: 32333359. doi:10.1007/s10753-020-01233-w
10. Stanzani G, Duchen MR, Singer M. The role of mitochondria in sepsis-induced cardiomyopathy. *Biochim Biophys Acta Mol Basis Dis*. 2019;1865(4):759–773. PMID: 30342158. doi:10.1016/j.bbadis.2018.10.011
11. Pierrakos C, Velissaris D, Bisdorff M, Marshall JC, Vincent JL. Biomarkers of sepsis: time for a reappraisal. *Critical Care*. 2020;24(1):287. PMID: 32503670. doi:10.1186/s13054-020-02993-5
12. Cecconi M, Evans L, Levy M, Rhodes A. Sepsis and septic shock. *Lancet*. 2018;392(10141):75–87. PMID: 29937192. doi:10.1016/s0140-6736(18)30696-2
13. Liu Q, Wu J, Zhang X, Wu X, Zhao Y, Ren J. Iron homeostasis and disorders revisited in the sepsis. *Free Radic Biol Med*. 2021;165:1–13. PMID: 33486088. doi:10.1016/j.freeradbiomed.2021.01.025
14. Fang X, Ardehali H, Min J, Wang F. The molecular and metabolic landscape of iron and ferroptosis in cardiovascular disease. *Nat Rev Cardiol*. 2022:1–17. PMID: 35788564; PubMed Central PMCID: PMCPMC9252571. doi:10.1038/s41569-022-00735-4
15. Brandtner A, Tymoszuk P, Nairz M, et al. Linkage of alterations in systemic iron homeostasis to patients' outcome in sepsis: a prospective study. *J Intensive Care*. 2020;8:76. PMID: 33014378. doi:10.1186/s40560-020-00495-8
16. Akkaş İ, Ince N, Sungur MA. Serum trace element and heavy metal levels in patients with sepsis. *Aging Male*. 2020;23(3):222–226. PMID: 32183594. doi:10.1080/13685538.2020.1740200
17. Xl L, Gy Z. Ferroptosis in sepsis: the mechanism, the role and the therapeutic potential. *Front Immunol*. 2022;13:956361. PMID: 35990689. doi:10.3389/fimmu.2022.956361
18. Stockwell BR. Ferroptosis turns 10: emerging mechanisms, physiological functions, and therapeutic applications. *Cell*. 2022;185(14):2401–2421. PMID: 35803244. doi:10.1016/j.cell.2022.06.003
19. Kong C, Ni X, Wang Y, et al. ICA69 aggravates ferroptosis causing septic cardiac dysfunction via STING trafficking. *Cell Death Discov*. 2022;8(1):187. PMID: 35397620. doi:10.1038/s41420-022-00957-y
20. Xiao Z, Kong B, Fang J, et al. Ferrostatin-1 alleviates lipopolysaccharide-induced cardiac dysfunction. *Bioengineered*. 2021;12(2):9367–9376. PMID: 34787054. doi:10.1080/21655979.2021.2001913
21. Wang X, Simayi A, Fu J, Zhao X, Xu G. Resveratrol mediates the miR-149/HMGB1 axis and regulates the ferroptosis pathway to protect myocardium in endotoxemia mice. *Am J Physiol Endocrinol Metab*. 2022;323(1):E21–e32. PMID: 35532075. doi:10.1152/ajpendo.00227.2021
22. Zou HX, Qiu BQ, Lai SQ, et al. Role of ferroptosis-related genes in Stanford type a aortic dissection and identification of key genes: new insights from bioinformatic analysis. *Bioengineered*. 2021;12(2):9976–9990. PMID: 34652258. doi:10.1080/21655979.2021.1988840
23. Banchereau R, Cepika AM, Banchereau J, Pascual V. Understanding human autoimmunity and autoinflammation through transcriptomics. *Annu Rev Immunol*. 2017;35:337–370. PMID: 28142321. doi:10.1146/annurev-immunol-051116-052225
24. Ren X, Wen W, Fan X, et al. COVID-19 immune features revealed by a large-scale single-cell transcriptome atlas. *Cell*. 2021;184(7):1895–913.e19. PMID: 33657410. doi:10.1016/j.cell.2021.01.053

25. O'Donoghue ML, Rosenson RS, Gencer B, et al. Small Interfering RNA to Reduce Lipoprotein(a) in Cardiovascular Disease. *N Engl J Med*. 2022. PMID: 36342163. doi:10.1056/NEJMoa2211023
26. Wang W, Xu H, Lin H, Molnar M, Ren H. The role of the cholinergic anti-inflammatory pathway in septic cardiomyopathy. *Int Immunopharmacol*. 2021;90:107160. PMID: 33243604. doi:10.1016/j.intimp.2020.107160
27. Dou J, Liu X, Yang L, Huang D, Tan X. Ferroptosis interaction with inflammatory microenvironments: mechanism, biology, and treatment. *Biomed Pharmacother*. 2022;155:113711. PMID: 36126457. doi:10.1016/j.biopha.2022.113711
28. Ni S, Yuan Y, Song S, Li X. A double-edged sword with a therapeutic target: iron and ferroptosis in immune regulation. *Nutr Rev*. 2022. PMID: 36130411. doi:10.1093/nutrit/nuac071
29. Zou HX, Qiu BQ, Zhang ZY, et al. Dysregulated autophagy-related genes in septic cardiomyopathy: comprehensive bioinformatics analysis based on the human transcriptomes and experimental validation. *Front Cardiovasc Med*. 2022;9:923066. PMID: 35983185. doi:10.3389/fcvm.2022.923066
30. He Y, Yuan H, Wu C, Xie Z. DISC: a highly scalable and accurate inference of gene expression and structure for single-cell transcriptomes using semi-supervised deep learning. *Genome Biol*. 2020;21(1):170. PMID: 32650816. doi:10.1186/s13059-020-02083-3
31. Zou HX, Qiu BQ, Lai SQ, et al. Iron metabolism and idiopathic pulmonary arterial hypertension: new insights from bioinformatic analysis. *Biomed Res Int*. 2021;2021:5669412. PMID: 34722766. doi:10.1155/2021/5669412
32. Zhou N, Bao J. FerrDb: a manually curated resource for regulators and markers of ferroptosis and ferroptosis-disease associations. *Database*. 2020;2020. PMID: 32219413. doi:10.1093/database/baaa021
33. Shen W, Song Z, Zhong X, et al. Sangerbox: a comprehensive, interaction-friendly clinical bioinformatics analysis platform. *iMeta*. 2022;1(3):e36. doi:10.1002/imt2.36
34. Yu G, Wang LG, Han Y, He QY. ClusterProfiler: an R package for comparing biological themes among gene clusters. *Omics*. 2012;16(5):284–287. PMID: 22455463. doi:10.1089/omi.2011.0118
35. Zhou K, Wu G, Li Y, et al. Protective effects of indomethacin and dexamethasone in a goat model with intrauterine balloon aortic valvuloplasty. *J Biomed Sci*. 2012;19(1):74. doi:10.1186/1423-0127-19-74
36. Wu B, Song H, Fan M, et al. Luteolin attenuates sepsis-induced myocardial injury by enhancing autophagy in mice. *Int J Mol Med*. 2020;45 (5):1477–1487. PMID: 32323750. doi:10.3892/ijmm.2020.4536
37. Boyd JH, Kan B, Roberts H, Wang Y, Walley KR. S100A8 and S100A9 mediate endotoxin-induced cardiomyocyte dysfunction via the receptor for advanced glycation end products. *Circ Res*. 2008;102(10):1239–1246. PMID: 18403730. doi:10.1161/circresaha.107.167544
38. Anwar-mohamed A, Zordoky BN, Aboutabl ME, El-Kadi AO. Alteration of cardiac cytochrome P450-mediated arachidonic acid metabolism in response to lipopolysaccharide-induced acute systemic inflammation. *Pharmacol Res*. 2010;61(5):410–418. PMID: 20045729. doi:10.1016/j.phrs.2009.12.015
39. Shi G, Xing L, Wu D, et al. A rare mutation of β(1)-adrenergic receptor affects sleep/wake behaviors. *Neuron*. 2019;103(6):1044–55.e7. PMID: 31473062. doi:10.1016/j.neuron.2019.07.026
40. Tucker NR, Chaffin M, Fleming SJ, et al. Transcriptional and cellular diversity of the human heart. *Circulation*. 2020;142(5):466–482. PMID: 32403949. doi:10.1161/circulationaha.119.045401
41. Miao Y, Tian L, Martin M, et al. Abstract 12937: single-cell transcriptomic analysis reveals developmentally impaired endocardial population in hypoplastic left heart syndrome. *Circulation*. 2020;142(Suppl_3):A12937–A. doi:10.1161/circ.142.suppl_3.12937
42. Yoo M, Shin J, Kim J, et al. DSigDB: drug signatures database for gene set analysis. *Bioinformatics*. 2015;31(18):3069–3071. PMID: 25990557. doi:10.1093/bioinformatics/btv313
43. Chen EY, Tan CM, Kou Y, et al. Enrichr: interactive and collaborative HTML5 gene list enrichment analysis tool. *BMC Bioinform*. 2013;14:128. PMID: 23586463. doi:10.1186/1471-2105-14-128
44. Kim S, Chen J, Cheng T, et al. PubChem in 2021: new data content and improved web interfaces. *Nucleic Acids Res*. 2021;49(D1):D1388–d95. PMID: 33151290. doi:10.1093/nar/gkaa971
45. Burley SK, Bhikadiya C, Bi C, et al. RCSB Protein Data Bank: powerful new tools for exploring 3D structures of biological macromolecules for basic and applied research and education in fundamental biology, biomedicine, biotechnology, bioengineering and energy sciences. *Nucleic Acids Res*. 2020;49(D1):D437–D51. doi:10.1093/nar/gkaa1038
46. Jumper J, Evans R, Pritzel A, et al. Highly accurate protein structure prediction with AlphaFold. *Nature*. 2021;596(7873):583–589. PMID: 34265844. doi:10.1038/s41586-021-03819-2
47. Li N, Wang W, Zhou H, et al. Ferritinophagy-mediated ferroptosis is involved in sepsis-induced cardiac injury. *Free Radic Biol Med*. 2020;160:303–318. PMID: 32846217. doi:10.1016/j.freeradbiomed.2020.08.009
48. Miotto G, Rossetto M, Di Paolo ML, et al. Insight into the mechanism of ferroptosis inhibition by ferrostatin-1. *Redox Biol*. 2020;28:101328. PMID: 31574461. doi:10.1016/j.redox.2019.101328
49. Rosenzweig R, Kumar V, Gupta S, et al. Estrogen receptor-β agonists modulate t-lymphocyte activation and ameliorate left ventricular remodeling during chronic heart failure. *Circ Heart Fail*. 2022;15(7):e008997. PMID: 35730443. doi:10.1161/circheartfailure.121.008997
50. Kumar V, Prabhu SD, Bansal SS. CD4(+) T-lymphocytes exhibit biphasic kinetics post-myocardial infarction. *Front Cardiovasc Med*. 2022;9:992653. PMID: 36093172. doi:10.3389/fcvm.2022.992653
51. Liu YC, Yu MM, Shou ST, Chai YF. Sepsis-induced cardiomyopathy: mechanisms and treatments. *Front Immunol*. 2017;8:1021. PMID: 28970829. doi:10.3389/fimmu.2017.01021
52. Xu S, Min J, Wang F. Ferroptosis: an emerging player in immune cells (News&Views). *Sci Bull*. 2021;2021:2731–2744.
53. Wang P, Lu YQ. Ferroptosis: a critical moderator in the life cycle of immune cells. *Front Immunol*. 2022;13:877634. PMID: 35619718. doi:10.3389/fimmu.2022.877634
54. Cao G, Zeng Y, Zhao Y, et al. H2S regulation of ferroptosis attenuates sepsis-induced cardiomyopathy. *Mol Med Rep*. 2022;26(5). PMID: 36102305. doi:10.3892/mmr.2022.12851
55. Jiang X, Stockwell BR, Conrad M. Ferroptosis: mechanisms, biology and role in disease. *Nat Rev Mol Cell Biol*. 2021;22(4):266–282. PMID: 33495651. doi:10.1038/s41580-020-00324-8
56. Ajoolabady A, Aslkhodapasandhokmabad H, Libby P, et al. Ferritinophagy and ferroptosis in the management of metabolic diseases. *Trends Endocrinol Metab*. 2021;32(7):444–462. PMID: 34006412. doi:10.1016/j.tem.2021.04.010
57. Qin X, Zhang J, Wang B, et al. Ferritinophagy is involved in the zinc oxide nanoparticles-induced ferroptosis of vascular endothelial cells. *Autophagy*. 2021;17(12):4266–4285. PMID: 33843441. doi:10.1080/15548627.2021.1911016

58. Zhang Z, Guo M, Li Y, et al. RNA-binding protein ZFP36/TTP protects against ferroptosis by regulating autophagy signaling pathway in hepatic stellate cells. *Autophagy*. 2020;16(8):1482–1505. PMID: 31679460. doi:10.1080/15548627.2019.1687985
59. Zhang X, Du L, Qiao Y, et al. Ferroptosis is governed by differential regulation of transcription in liver cancer. *Redox Biol*. 2019;24:101211. PMID: 31108460. doi:10.1016/j.redox.2019.101211
60. Yang WS, Stockwell BR. Ferroptosis: death by Lipid Peroxidation. *Trends Cell Biol*. 2016;26(3):165–176. PMID: 26653790. doi:10.1016/j.tcb.2015.10.014
61. Park MW, Cha HW, Kim J, et al. NOX4 promotes ferroptosis of astrocytes by oxidative stress-induced lipid peroxidation via the impairment of mitochondrial metabolism in Alzheimer's diseases. *Redox Biol*. 2021;41:101947. PMID: 33774476. doi:10.1016/j.redox.2021.101947
62. Liu N, Liang Y, Wei T, et al. The role of ferroptosis mediated by NRF2/ERK-regulated ferritinophagy in CdTe QDs-induced inflammation in macrophage. *J Hazard Mater*. 2022;436:129043. PMID: 35525219. doi:10.1016/j.jhazmat.2022.129043
63. Yi J, Zhu J, Wu J, Thompson CB, Jiang X. Oncogenic activation of PI3K-AKT-mTOR signaling suppresses ferroptosis via SREBP-mediated lipogenesis. *Proc Natl Acad Sci U S A*. 2020;117(49):31189–31197. PMID: 33229547. doi:10.1073/pnas.2017152117
64. Xing G, Meng L, Cao S, et al. PPARα alleviates iron overload-induced ferroptosis in mouse liver. *EMBO Rep*. 2022;23(8):e52280. PMID: 35703725. doi:10.15252/embr.202052280
65. Xu M, Tao J, Yang Y, et al. Ferroptosis involves in intestinal epithelial cell death in ulcerative colitis. *Cell Death Dis*. 2020;11(2):86. PMID: 32015337. doi:10.1038/s41419-020-2299-1
66. Li Y, Cao Y, Xiao J, et al. Inhibitor of apoptosis-stimulating protein of p53 inhibits ferroptosis and alleviates intestinal ischemia/reperfusion-induced acute lung injury. *Cell Death Differ*. 2020;27(9):2635–2650. PMID: 32203170. doi:10.1038/s41418-020-0528-x
67. Yuan S, Wei C, Liu G, et al. Sorafenib attenuates liver fibrosis by triggering hepatic stellate cell ferroptosis via HIF-1α/SLC7A11 pathway. *Cell Prolif*. 2022;55(1):e13158. PMID: 34811833. doi:10.1111/cpr.13158
68. Zhou B, Liu J, Kang R, Klionsky DJ, Kroemer G, Tang D. Ferroptosis is a type of autophagy-dependent cell death. *Semin Cancer Biol*. 2020;66:89–100. PMID: 30880243. doi:10.1016/j.semcancer.2019.03.002
69. Ma H, Wang X, Ha T, et al. MicroRNA-125b prevents cardiac dysfunction in polymicrobial sepsis by targeting TRAF6-mediated nuclear factor κB Activation and p53-mediated apoptotic signaling. *J Infect Dis*. 2016;214(11):1773–1783. PMID: 27683819. doi:10.1093/infdis/jiw449
70. Yu Y, Ou-Yang WX, Zhang H, et al. MiR-125b enhances autophagic flux to improve septic cardiomyopathy via targeting STAT3/HMGB1. *Exp Cell Res*. 2021;409(2):112842. PMID: 34563514. doi:10.1016/j.yexcr.2021.112842
71. Zhao H, Zhang M, Zhou F, et al. Cinnamaldehyde ameliorates LPS-induced cardiac dysfunction via TLR4-NOX4 pathway: the regulation of autophagy and ROS production. *J Mol Cell Cardiol*. 2016;101:11–24. PMID: 27838370. doi:10.1016/j.yjmcc.2016.10.017
72. Xia C, Dong R, Chen C, Wang H, Wang DW. Cardiomyocyte specific expression of Acyl-coA thioesterase 1 attenuates sepsis induced cardiac dysfunction and mortality. *Biochem Biophys Res Commun*. 2015;468(4):533–540. PMID: 26518651. doi:10.1016/j.bbrc.2015.10.078
73. Yao Y, Sun F, Lei M. miR-25 inhibits sepsis-induced cardiomyocyte apoptosis by targetting PTEN. *Biosci Rep*. 2018;38(2). PMID: 29440462. doi:10.1042/bsr20171511
74. Ehrman RR, Sullivan AN, Favot MJ, et al. Pathophysiology, echocardiographic evaluation, biomarker findings, and prognostic implications of septic cardiomyopathy: a review of the literature. *Critical Care*. 2018;22(1):112. PMID: 29724231. doi:10.1186/s13054-018-2043-8
75. Lv X, Wang H. Pathophysiology of sepsis-induced myocardial dysfunction. *Mil Med Res*. 2016;3:30. PMID: 27708836. doi:10.1186/s40779-016-0099-9
76. Pinto AR, Paolicelli R, Salimova E, et al. An abundant tissue macrophage population in the adult murine heart with a distinct alternatively-activated macrophage profile. *PLoS One*. 2012;7(5):e36814. PMID: 22590615. doi:10.1371/journal.pone.0036814
77. Nicolás-ávila JA, Pena-Couso L, Muñoz-Cánoves P, Hidalgo A. Macrophages, metabolism and heterophagy in the heart. *Circ Res*. 2022;130(3):418–431. PMID: 35113662. doi:10.1161/circresaha.121.319812
78. Wang L, Li Y, Wang X, et al. GDF3 protects mice against sepsis-induced cardiac dysfunction and mortality by suppression of macrophage pro-inflammatory phenotype. *Cells*. 2020;9(1). PMID: 31947892. doi:10.3390/cells9010120
79. Zhang J, Wang M, Ye J, et al. The Anti-inflammatory mediator resolvin e1 protects mice against lipopolysaccharide-induced heart injury. *Front Pharmacol*. 2020;11:203. PMID: 32256344. doi:10.3389/fphar.2020.00203
80. Guo L, Shen S, Rowley JW, et al. Platelet MHC class I mediates CD8+ T-cell suppression during sepsis. *Blood*. 2021;138(5):401–416. PMID: 33895821. doi:10.1182/blood.2020008958
81. Guo L, Meng M, Wei Y, et al. Protective Effects of Live Combined B. subtilis and E. faecium in polymicrobial sepsis through modulating activation and transformation of macrophages and mast cells. *Front Pharmacol*. 2018;9:1506. PMID: 30719003. doi:10.3389/fphar.2018.01506
82. Ver Elst KM, Spapen HD, Nguyen DN, Garbar C, Huyghens LP, Gorus FK. Cardiac troponins I and T are biological markers of left ventricular dysfunction in septic shock. *Clin Chem*. 2000;46(5):650–657. PMID: 10794747. doi:10.1093/clinchem/46.5.650
83. Nedeva C. Inflammation and cell death of the innate and adaptive immune system during sepsis. *Biomolecules*. 2021;11(7). PMID: 34356636. doi:10.3390/biom11071011
84. Sun K, Li YY, Jin J. A double-edged sword of immuno-microenvironment in cardiac homeostasis and injury repair. *Curr Signal Transduct Ther*. 2021;6(1):79. PMID: 33612829. doi:10.1038/s41392-020-00455-6
85. van der Poll T, van de Veerdonk FL, Scicluna BP, Netea MG. The immunopathology of sepsis and potential therapeutic targets. *Nat Rev Immunol*. 2017;17(7):407–420. PMID: 28436424. doi:10.1038/nri.2017.36
86. Bai T, Hu X, Zheng Y, Wang S, Kong J, Cai L. Resveratrol protects against lipopolysaccharide-induced cardiac dysfunction by enhancing SERCA2a activity through promoting the phospholamban oligomerization. *Am J Physiol Heart Circ Physiol*. 2016;311(4):H1051–h62. PMID: 27591219. doi:10.1152/ajpheart.00296.2016
87. Hao E, Lang F, Chen Y, et al. Resveratrol alleviates endotoxin-induced myocardial toxicity via the Nrf2 transcription factor. *PLoS One*. 2013;8(7):e69452. PMID: 23894482. doi:10.1371/journal.pone.0069452
88. Shang X, Lin K, Yu R, et al. Resveratrol protects the myocardium in sepsis by activating the phosphatidylinositol 3-kinases (PI3K)/AKT/mammalian target of rapamycin (mtor) pathway and inhibiting the nuclear factor-κB (NF-κB) signaling pathway. *Med Sci Monit*. 2019;25:9290–9298. PMID: 31806860. doi:10.12659/msm.918369
89. Sebai H, Sani M, Aouani E, Ghanem-Boughanmi N. Cardioprotective effect of resveratrol on lipopolysaccharide-induced oxidative stress in rat. *Drug Chem Toxicol*. 2011;34(2):146–150. PMID: 21314464. doi:10.3109/01480545.2010.494666